



1 **Spatio-temporal changes in cryoconite community, isotopic, and elemental composition**  
2 **over the ablation season of an alpine glacier**

3 **Tereza Novotná Jaroměřská<sup>1</sup>, Roberto Ambrosini<sup>2</sup>, Dorota Richter<sup>3</sup>, Mirosława**  
4 **Pietryka<sup>3</sup>, Przemysław Niedzielski<sup>4</sup>, Juliana Souza-Kasprzyk<sup>4</sup>, Piotr Klimaszyk<sup>5</sup>, Andrea**  
5 **Franzetti<sup>6</sup>, Francesca Pittino<sup>7</sup>, Lenka Vondrovicová<sup>8</sup>, Tyler Kohler<sup>1</sup>, and Krzysztof**  
6 **Zawierucha<sup>9\*</sup>**

7 *<sup>1</sup>Department of Ecology, Faculty of Science, Charles University, Praha, Czech Republic*

8 *<sup>2</sup>Department of Environmental Science and Policy, University of Milan, Milan, Italy*

9 *<sup>3</sup>Department of Botany and Plant Ecology, Wrocław University of Environmental and Life*  
10 *Science, Wrocław, Poland*

11 *<sup>4</sup>Department of Analytical Chemistry, Faculty of Chemistry, Adam Mickiewicz University,*  
12 *Poznań, Poland*

13 *<sup>5</sup>Department of Water Protection, Faculty of Biology, Adam Mickiewicz University, Poznań,*  
14 *Poland*

15 *<sup>6</sup>Department of Earth and Environmental Sciences, University of Milano-Bicocca, Milan, Italy*

16 *<sup>7</sup>Biodivers. Conserv. Biology, Swiss Federal Research Institute WSL, Birmensdorf, Switzerland*

17 *<sup>8</sup>Institute of Geochemistry, Mineralogy and Mineral Resources, Faculty of Science, Charles*  
18 *University, Prague, Czech Republic*

19 *<sup>9</sup>Department of Animal Taxonomy and Ecology, Faculty of Biology, Adam Mickiewicz*  
20 *University, Poznań, Poland*

21 \* Correspondence: Krzysztof Zawierucha ([k.p.zawierucha@gmail.com](mailto:k.p.zawierucha@gmail.com))



22 **Abstract:** Cryoconite holes (water-filled reservoirs) on glacier surfaces are important  
23 biodiversity hotspots and biogeochemical factories within terrestrial cryosphere. In this study,  
24 we collected cryoconite from the ablation zone of the Forni Glacier (Central Italian Alps) over  
25 the whole ablation season. We aimed to describe spatial and temporal patterns in: (i) biomass  
26 and community structure of photoautotrophs (cyanobacteria, diatoms, and eukaryotic green  
27 algae) and invertebrates; (ii) carbon and nitrogen stable isotopic composition of invertebrates  
28 and their potential food; and (iii) the organic matter content and general elemental composition  
29 of cryoconite. Structure and biomass of cryoconite biota showed spatio-temporal changes over  
30 the season. Dominant cyanobacteria were Oscillatoriaceae and Leptolyngbyaceae, while  
31 dominant eukaryotic green algae were Mesotaeniaceae and Chlorellaceae. Eukaryotic green  
32 algae dominated in the upper part of the ablation zone, while a seasonal shift from algae- to  
33 cyanobacteria-dominated communities was observed in the lower part. Some taxa of  
34 photoautotrophs appeared only during specific sampling days. Dominant grazers were  
35 tardigrades (*Cryobiotus klebelsbergi*). The biomass of tardigrades in the upper part was  
36 significantly related to the biomass of eukaryotic green algae indicating that algal communities  
37 are likely controlled by grazing. The  $\delta^{13}\text{C}$  of tardigrades followed fluctuations of  $\delta^{13}\text{C}$  in organic  
38 matter. We did not observe spatial and temporal changes in the general elemental composition  
39 of cryoconite. Thus, changes in community structure and biomass are likely dependent on the  
40 interplay between phenology, stochastic events (e.g. rainfall), top-down, or bottom-up controls.  
41 Our study shows that understanding the ecology of biota in cryoconite holes requires a spatially  
42 explicit and seasonal approach.

43 **Keywords:** top-down control, Forni Glacier, Tardigrada, stable isotopes, phenology,  
44 supraglacial habitats

45



46 **1. Introduction**

47 Studies on changes in the distribution, structure, and biomass of organisms in space and time  
48 are important for understanding the phenology and resources use of species and their responses  
49 to environmental shifts (Post and Stenseth, 1999; Sommers et al., 2019; Vecchi et al., 2021;  
50 Walther et al., 2002; Winkel et al., 2022). Glaciers and ice sheets are one of the fastest-changing  
51 biomes on Earth (Anesio and Laybourn-Parry, 2012; Zemp et al., 2006). The biological activity  
52 on the glacier surface (supraglacial) can affect the surface albedo (reflection of solar radiation)  
53 with potential implications to glacier melt dynamic (e.g. Stibal et al., 2012a; Yallop et al., 2012).  
54 Understanding the controls on the biodiversity, and phenology of glacial biota is therefore  
55 crucial for modelling how climate changes may alter glacial ecosystems (Anesio and Laybourn-  
56 Parry, 2012; Gobbi et al., 2021; Stibal et al., 2012a).

57 Most biological processes within the supraglacial environment occur during the ablation  
58 season when air temperature rises, day length is extended, and snow melts (Cameron et al.,  
59 2012; Senese et al., 2012; Stibal et al., 2012a). During that time, glacier surfaces provide liquid  
60 water and suitable conditions for the activity of myriad organisms from bacteria to invertebrates  
61 (e.g. Cameron et al., 2012; Shain et al., 2021; Zawierucha et al., 2018, 2020). On glaciers, the  
62 highest biodiversity is found in cryoconite holes, which are small water-filled depressions on  
63 the glacier surface formed by a dark sediment (the cryoconite) that lowers the albedo of the  
64 glacier surface and melts into the ice (Cameron et al., 2012; Takeuchi et al., 2001a; Wharton et  
65 al., 1985). Due to their pond-like structure, cryoconite holes harbour a unique community of  
66 organisms from microbes to minute invertebrates (Edwards et al., 2013; Franzetti et al., 2017;  
67 Poniecka et al., 2020; Zawierucha et al., 2019a).

68 Although biological communities on glaciers have been intensively studied over recent  
69 years, changes in the community structure of cryoconite over the ablation season have been  
70 minimally investigated (e.g. Musilova et al., 2015; Pittino et al., 2018; Takeuchi 2013; Winkel



71 et al., 2021), and some of these studies have brought contrasting results. For example, Pittino  
72 et al. (2018) showed that the supraglacial microbial community structure in the Alps changed  
73 over the ablation season from a dominance of cyanobacteria to heterotrophic bacteria.  
74 Conversely, on an Arctic glacier, Musilova et al. (2015) showed that community structure  
75 appeared to be stable over the season. Moreover, studies considering the biomass of different  
76 taxa from cryoconite holes are scarce and do not include seasonal observations (e.g. Buda et  
77 al., 2020) although biomass estimation is critical from a mass-balance perspective of  
78 biogeochemistry.

79 It is known that microinvertebrates can play an important role as consumers in polar  
80 ecosystems (Almela et al., 2019; Shaw et al., 2018; Velázquez et al., 2017). However, their role  
81 in the supraglacial trophic network remains unclear (Novotná Jaroměřská et al., 2021;  
82 Zawierucha et al., 2018), and our understanding of the interactions between microbial  
83 communities and their consumers on glaciers is scant. Even though some studies have  
84 investigated the ecology and community structure of biota in cryoconite together with the  
85 potential food of tardigrades by various methods (Vonnahme et al., 2016; Zawierucha et al.,  
86 2022), evidence related to their potential ecological and trophic roles, including possible top-  
87 down control of the cryoconite ecosystem, remains limited.

88 Until now, seasonal patterns in the community structure and biomass of both  
89 photoautotrophs and consumers in cryoconite on alpine glaciers have never been studied. Such  
90 missing information on their seasonal evolution prevents the estimation and understanding of  
91 (i) biological diversity on glaciers, since some taxa may appear only in a particular period  
92 during the ablation season (Pittino et al., 2018); (ii) trophic links, which are difficult to resolve  
93 in snapshot studies (e.g. Zawierucha et al., 2018); and (iii) the blooming of photoautotrophs in  
94 cryoconite and the consequent increase of biological activity which may spur supraglacial melt  
95 (Williamson et al., 2020). Moreover, seasonal differences in the community structure of



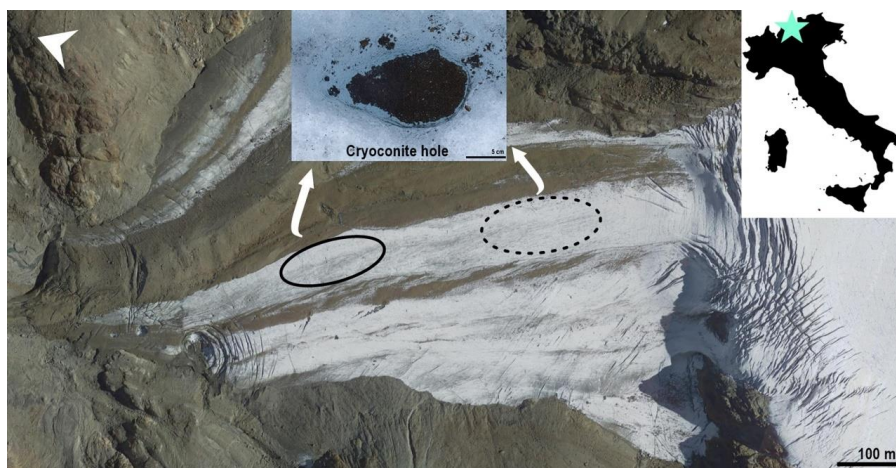
96 cryoconite organisms, especially in the production and availability of organic matter (OM), may  
97 affect the composition and nutritional content of glacier meltwater, which is one of the major  
98 sources of water to the proglacial (in front of the glacier) areas and downstream systems in  
99 alpine and polar regions (Bagshaw et al., 2013; Colombo et al., 2019; Fountain et al., 2004;  
100 MacDonell and Fitzsimons, 2008).

101 In this study, we investigated the community structure and the biomass of photoautotrophs  
102 and consumers, the isotopic composition of consumers and OM in cryoconite, and the general  
103 elemental composition of cryoconite on the Forni Glacier, one of the most extensively studied  
104 glacier in the Alps (e.g. Azzoni et al., 2016; Citterio et al., 2007; Franzetti et al., 2017; Pittino  
105 et al., 2018; Senese et al., 2012, 2020; Zawierucha et al., 2019a, 2021, 2022). We tested three  
106 main hypotheses: (i) seasonal changes in the community structure and biomass of  
107 photoautotrophs on the Forni Glacier are reflected in the community structure and biomass of  
108 consumers; (ii) seasonal changes in the general elemental composition of cryoconite are directly  
109 connected with the community structure and biomass of photoautotrophs and consumers; (iii)  
110 carbon and nitrogen stable isotopic composition of OM and consumers in cryoconite changes  
111 during the ablation season and mirrors seasonal changes in the cryoconite community structure.

## 112 **2. Material and methods**

### 113 **2.1 Study site and sampling**

114 The Forni Glacier (Fig. 1) is a valley type mountain glacier located in the Ortles–Cevedale  
115 group (Stelvio National Park, Central Italian Alps). As one of the largest glaciers in Italy with  
116 an area of about 10.83 km<sup>2</sup>, the Forni Glacier is diminishing rapidly every year. The elevation  
117 of Forni Glacier ranges between 2600 and 3670 m a. s. l. (Senese et al., 2018). Cryoconite holes  
118 are located on the tongue of the glacier. The lower part of the tongue is characterized by a mild  
119 slope with small boulders and coarse grain debris on the glacier surface. The upper part of the  
120 tongue is flat with visible patches of scattered cryoconite.



121

122 **Figure 1.** Location of sampling sites at the Forni Glacier. Solid oval indicates lower sampling  
123 sites, dotted oval indicates upper sampling sites. Source: Google Earth, version 9.172.0.0 -  
124 WebAssembly with threads (Forni Glacier 24.09.2021). © Google Earth.

125 Cryoconite samples were collected from the lower (approx. 2650 m a. s. l.) and the upper part  
126 (approx. 2700 m a. s. l.) of the ablation area (the area where the ice mass loss exceeds its  
127 increase) below the seracs that connect the ablation and the accumulation area (the area where  
128 the ice accrual exceeds its decrease) of the glacier (Senese et al., 2012). Horizontal distance  
129 between upper and lower sampling site was 250–300 metres. Cryoconite was collected from  
130 the bottom of cryoconite holes in five sampling campaigns during the 2019 ablation season  
131 (July 4<sup>th</sup> and 26<sup>th</sup>, August 15<sup>th</sup> and 30<sup>th</sup>, and September 19<sup>th</sup>). Samples were collected with an  
132 aseptic stainless spoon and transferred into 50 mL plastic test tubes. During each sampling  
133 campaign, cryoconite was collected from at least 5 holes to create one pooled sample at each  
134 part of the ablation zone. After collection, cryoconite was frozen and transported to a laboratory  
135 at the Adam Mickiewicz University, Poznań (Poland). Thereafter, material from each pooled  
136 sample was well mixed and split for subsequent analyses (see details below).

137

138



## 139 **2.2 Identification and quantification of photoautotrophs**

140 Morphological observations were conducted using a Nikon Eclipse TE2000-S digital  
141 microscope equipped with a Nikon DS-Fi1 camera under the magnification 100×.  
142 Morphometric analysis of species was conducted using NIS image analysis software.  
143 Identification of cyanobacteria, diatoms (only specimens with well-preserved, visible  
144 chloroplasts were considered for analyses), and eukaryotic green algae followed Hindak (1996),  
145 Coesel and Meesters (2007), John and Rindi (2015), Komárek and Anagnostidis (2005), and  
146 Krammer and Lange-Bertalot (1986, 1991a, 1991b). The taxonomy and nomenclature of  
147 cyanobacteria, diatoms, and eukaryotic green algae were confirmed based on Algaebase  
148 (<https://www.algaebase.org/>).

149 For quantitative analyses, each sample was analysed in 10 repetitions. For each repetition, 200  
150 µL of analysed sample water was placed on a glass slide under a coverslip and the number of  
151 photoautotrophs were counted. Cells of photoautotrophs were counted in strips and the mean  
152 value of strips on a slide was 20. The “calculation units”, namely individual cells or 100 µm  
153 filaments, were counted. Fifty specimens from each species were measured, the mean cell size  
154 or filaments were calculated with the reference to their similarity to geometric shapes according  
155 to Hutorowicz (2006). The resulting data (i.e., mean volume and number of cells in given  
156 volume) were used to calculate the biomass of individual taxa (Hutorowicz, 2006). The algal  
157 biomass is calculated by assuming that the algal cell density is 1.0 g/cm<sup>3</sup>, then the algal biomass  
158 is equal to its volume.

## 159 **2.3 Identification and quantification of top consumers**

160 In the laboratory, 6 mL of cryoconite were analysed after slow melting in the fridge at 3 °C to  
161 avoid a heat shock to consumers. Tardigrades were identified using the original description of  
162 Mihelcic (1959), the redescription in Dastych et al. (2003), and previous description of  
163 microinvertebrates in cryoconite on the Forni Glacier (Zawierucha et al., 2019a). For the



164 extraction of consumers, cryoconite was placed into a Petri dish ( $\varnothing$  8.5 cm) and scanned for  
165 microfauna using a stereomicroscope (Olympus BZ51). On the bottom of each Petri dish,  
166 parallel thin lines were drawn with a black marker every 5 mm to increase the precision of  
167 scanning (5 mm corresponds to a visible image at 30 $\times$  magnification). All tardigrades were  
168 extracted with small shovels and counted. Petri dishes were placed on the ice pad to provide  
169 cooling for glacier invertebrates during the extraction. The density of animals was calculated  
170 per 1 cm<sup>3</sup> and per 1 g of dry cryoconite.

#### 171 **2.4 Biomass of tardigrades**

172 For the calculation of biomass of tardigrades, body length and width of individuals were  
173 manually measured on photographs taken by the Quick PHOTO Camera 3.0 software (Promicra,  
174 Prague, Czech Republic) under an Olympus BX53. Animals not suitable for measurements  
175 (broken, bended) were not measured. Mass (wet mass (WM)) of each specimen was calculated  
176 based on the formula of Hallas and Yates (1972): if body length (L) and width (D) were 4:1; WM  
177 =  $L^3 \times 0.051 \times 10^{-6}$ , or 5:1; WM =  $L^3 \times 0.033 \times 10^{-6}$ .

#### 178 **2.5 Organic matter in cryoconite**

179 The amount of organic matter in cryoconite was measured as a percentage of weight loss  
180 through combustion (i.e., loss on ignition, LOI) at 550 °C for 3 h following drying at 50 °C for  
181 24 h (Wang et al., 2011). The method was previously used in studies on organic matter content  
182 in cryoconite worldwide (Rozwalak et al., 2022).

#### 183 **2.6 General elemental composition of cryoconite**

##### 184 **2.6.1 Procedure**

185 For the general elemental composition of cryoconite, combusted samples (without organic  
186 matter) of cryoconite were used. The elements analysed were Al, As, B, Ba, Be, Bi, Ca, Cd, Ce,



187 Co, Cr, Cu, Dy, Er, Eu, Fe, Ga, Gd, Ge, Hf, Hg, Ho, K, La, Li, Lu, Mg, Mn, Mo, Na, Nb, Nd,  
188 Ni, Os, P, Pb, Pr, Rb, Re, Rh, Ru, Sb, Sc, Se, Si, Sm, Sn, Sr, Ta, Tb, Te, Th, Ti, Tl, Tm, V, W,  
189 Y, Yb, Zn, and Zr. Before starting the analyses, samples were dried at  $+35 \pm 2$  °C in an electric  
190 oven (Thermocenter, Salvislab, Switzerland). Then, 200 mg (with the accuracy  $\pm 1$  mg) of each  
191 sample were extracted in closed Teflon containers with 5 mL of 65% nitric acid (Sigma-  
192 Aldrich, USA) using a Mars 6 (Mars 6 Xpress, CEM USA) microwave digestion system.  
193 Thereafter, samples were filtered and refilled to a total volume of 15 mL with Milli-Q water  
194 (Direct-Q system, Millipore, Germany). Just before the analysis, each sample was diluted 20  
195 times with Milli-Q water.

#### 196 **2.6.2 Instrumentation**

197 The concentration of elements was determined by a PlasmaQuant MS Q (AnalytikJena,  
198 Germany) inductively coupled plasma mass spectrometry. The instrumental conditions were:  
199 plasma gas flow  $9.0 \text{ L min}^{-1}$ , auxiliary gas flow  $1.5 \text{ L min}^{-1}$ , nebulizer gas flow  $1.05 \text{ L min}^{-1}$ ,  
200 Radio Frequency (RF) power 1.35 kW, signal has been measured in 5 replicates (20 scans each).  
201 The mass interferences were reduced using the integrated Collision Reaction Cell (iCRC)  
202 working sequentially in three modes: without gas addition, with hydrogen as reaction gas and  
203 with helium as collision gas.

#### 204 **2.6.3 Analytical method validation**

205 The uncertainty for the total analytical procedure was below 20 %. Expanded uncertainty with  
206 coverage factor of  $k = 2$  (approximate 95% confidence) was calculated for all analytical steps  
207 including sample preparation and instrumental analysis. The detection limits were calculated as  
208 the concentration corresponding to the signal equal to three times the standard deviation of the  
209 blank signal in the level of  $0.001 \text{ mg kg}^{-1}$  of dry weight (DW). The traceability was checked by  
210 the analysis of Standard Reference Materials (SRMs) NCS DC73349 (bush branches and



211 leaves, NCS Testing Technology, China), IAEA-405 (estuarine sediments, International  
212 Atomic Energy Agency, IAEA, Austria), SRM 2709a (San Joaquin soil, National Institute of  
213 Standards and Technology, USA); BCR-667 (estuarine sediments, Institute for Reference  
214 Materials and Measurements, Belgium). Following the quality control requirements, the  
215 analysis was considered valid when the results found for CRMs (certified reference material)  
216 presented recovery were between 80% and 120%. Additionally, the standard addition method  
217 was provided for elements with not certified values.

## 218 **2.7 Analyses of carbon and nitrogen stable isotopes**

### 219 **2.7.1 Preparation of tardigrades**

220 For the analyses of tardigrades, cryoconite was melted (Sect. 2.3) and tardigrades were collected  
221 using a glass Pasteur pipette according to Novotná Jaroměřská et al. (2021). Thereafter, samples  
222 were stored at  $-20\text{ }^{\circ}\text{C}$  until further processing started. After all samples of tardigrades were  
223 prepared, they were melted, and each individual was cleaned at least twice in a drop of distilled  
224 water under a light microscope (Leica DM750) from superficial mineral and organic particles.  
225 Thereafter, all tardigrades were transferred into pre-weighted tin capsules (Elemental  
226 Microanalysis,  $8 \times 5\text{ mm}$ , D1013) using a glass Pasteur pipette. Afterwards, all samples were  
227 stored overnight at  $-20\text{ }^{\circ}\text{C}$  and at  $-80\text{ }^{\circ}\text{C}$  for 1 h before the lyophilization started. The duration  
228 of lyophilization was 2 h. Thereafter, samples were weighted (Mettler Toledo Excellence Plus  
229 XP6; linearity = 0.0004 mg) and tin capsules were closed, wrapped, and analysed for stable  
230 nitrogen ( $\delta^{15}\text{N}$ ) and carbon ( $\delta^{13}\text{C}$ ) isotopic composition. To avoid carbon contamination, all  
231 work was conducted using nitrile gloves. Besides tardigrades, we found a few individuals of  
232 rotifers in cryoconite. Nevertheless, their occurrence in our samples was very low (few or no  
233 specimens among tens or hundreds of tardigrades). Therefore, rotifers were not further  
234 analysed.

### 235 **2.7.2 Preparation of cryoconite**



236 For analyses of cryoconite, all animals were removed using glass Pasteur pipettes and samples  
237 were frozen at  $-20\text{ }^{\circ}\text{C}$  before further processing started. Thereafter, material was melted and  
238 homogenized using an agate pestle and mortar and dried on a Petri dish at  $45\text{ }^{\circ}\text{C}$  for 14 h. To  
239 avoid any contamination between samples, we partially covered all Petri dishes by an  
240 aluminium film during the drying.

241 For analyses of  $\delta^{15}\text{N}$  in organic matter, the dry cryoconite was transferred without any other  
242 preparation to pre-weighted tin capsules (Costech,  $9 \times 5\text{ mm}$ , product code 41077) and  
243 weighted. All samples were prepared in 3 replicates with an average weight  $\sim 29.93\text{ mg}$  of dry  
244 material. Before analyses, samples were stored in a desiccator for 10 d.

245 For analyses of  $\delta^{13}\text{C}$  in OM,  $\sim 0.73\text{ mg}$  of dry material was transferred into pre-weighted silver  
246 capsules (Elemental Microanalysis,  $8 \times 5\text{ mm}$ , D2008) and carbonates were dissolved using  
247 10% HCl moistened with  $\text{dH}_2\text{O}$ . The acid was pipetted into capsules following additions of 15,  
248 15, 20, 50, 100  $\mu\text{L}$  with drying after each addition equal or up to 50  $\mu\text{L}$  according to Brodie et  
249 al. (2011) with the modification after Vindušková et al. (2019). After the last acid addition,  
250 samples were left drying at  $50\text{ }^{\circ}\text{C}$  for 19 h. After drying, silver capsules were inserted into tin  
251 capsules and put into a desiccator for 10 d.

### 252 **2.7.3 Stable isotopic analyses**

253 Analyses of  $\delta^{13}\text{C}$  and  $\delta^{15}\text{N}$  in all samples were performed using a Flash 2000 elemental analyser  
254 (ThermoFisher Scientific, Bremen, Germany) as described in Novotná Jaroměřská et al. (2021).  
255 Released gasses ( $\text{NO}_x$ ,  $\text{CO}_2$ ) separated in a GC (gas chromatography) column were transferred  
256 to an isotope-ratio mass spectrometer Delta V Advantage (ThermoFisher Scientific, Germany)  
257 through a capillary by Continuous Flow IV system (ThermoFisher Scientific, Germany). The  
258 stable isotope values were expressed in standard delta notation ( $\delta$ ) with samples measured  
259 relative to Pee Dee Belemnite for carbon isotopes and atmospheric  $\text{N}_2$  for nitrogen isotopes and  
260 normalized to a regression curve based on international standards IAEA-CH-6, IAEA-CH-3,



261 IAEA 600 (IAEA, Vienna) for carbon and IAEA-N-2, IAEA-N-1, IAEA-NO-3 (IAEA, Vienna)  
262 for nitrogen. The regression curve of the total gas for analyses of cryoconite was based on the  
263 international standard Soil Standard Clay OAS (Elemental Microanalysis, UK). Analytical  
264 precision as a long reproducibility for standards was within  $\pm 0.03$  ‰ for  $\delta^{13}\text{C}$  and  $\pm 0.02$  ‰  
265 for  $\delta^{15}\text{N}$ .

266 The  $\delta^{13}\text{C}$  and  $\delta^{15}\text{N}$  of OM in cryoconite were used as a reference to the isotopic  
267 composition of potential food source for the tardigrades. The  $\delta^{13}\text{C}$  of OM in cryoconite was  
268 used in all statistical analyses.

## 269 **2.8 Statistical analyses**

270 The variations in the biomass of photoautotrophs along the season were investigated by linear  
271 models that included sampling date, elevation (lower or upper part of the ablation zone,  
272 dichotomous factor), and their interaction. Biomass values were log-transformed before  
273 analyses to improve the model fit and statistical significance was assessed by a permutation  
274 approach to account for small deviations from model assumptions. Similarly, the variation of  
275 tardigrade biomass was related to the biomass of photoautotrophs by a linear model that also  
276 included the elevation and their interaction as predictors.

277 The relative biomass of photoautotrophic groups (cyanobacteria, diatoms, and eukaryotic  
278 green algae) was investigated with a redundancy analysis (RDA) on Hellinger-transformed  
279 relative biomass. Stable isotopic values and elemental composition of cryoconite were analysed  
280 using (RDA). Stable isotopic values were also compared between parts of the ablation zones  
281 by univariate statistical tests (t-tests) whose significance was assessed with a permutation  
282 approach because data slightly deviated from the assumptions of parametric tests.

## 283 **3. Results**

### 284 **3.1 The community structure and biomass of consumers and photoautotrophs**



285 Dominant invertebrates found in cryoconite were tardigrades, represented by a single species,  
 286 *Cryobiotus klebelsbergi*. Among hundreds of tardigrades, only a few bdelloid rotifers were  
 287 detected. The most abundant families of: (i) cyanobacteria were Oscillatoriaceae and  
 288 Leptolyngbyaceae, (ii) diatoms were Stephanodiscaceae, Aulacoseiraceae, and Bacillariaceae,  
 289 and (iii) eukaryotic green algae were Mesotaeniaceae, Chlorellaceae, and Oocystaceae (Table  
 290 1, Table S1).

Sample		4.7		26.7		15.8		30.8		19.9	
Elevation		Lower	Upper								
Cyanobacteria	<i>Chroococcus</i> sp.										
	<i>Phormidium</i> sp.										
	<i>Leptolyngbya</i> sp. 1										
	<i>Leptolyngbya</i> sp. 2										
	<i>Pseudanabaena</i> sp.										
Eukaryotic green algae	<i>Cylindrocapsa brebbisoni</i> De Bary f.										
	<i>cryophila</i> Kol										
	<i>Chlorella</i> sp.										
	<i>Mesotaenium</i> sp.										
	<i>Trachiscia granulata</i> Hansg.										
	<i>Trachiscia</i> sp.										
	coccoid green algae										
Diatoms	<i>Fragilaria</i> sp.										
	<i>Nitzschia</i> sp. 1										
	<i>Nitzschia</i> sp. 2										
	<i>Nitzschia</i> sp. 3										
	<i>Cyclotella</i> sp.										
	<i>Pinnularia</i> sp. 2										
	<i>Pinnularia</i> sp. 1										
	<i>Eunotia</i> sp.										
	<i>Achnanthes</i> sp.										
	<i>Diatoma</i> sp.										
	<i>Suriella</i> sp.										
	<i>Aulacoseira granulata</i> Simonsen										
Unidentified 1											
Unidentified 2											

291

292 **Table 1.** Presence (dark colour) and absence (light colour) of specific taxa of cyanobacteria,  
 293 diatoms, and eukaryotic green algae in samples from the upper (U) and lower (L) part of the  
 294 ablation zone at the alpine glacier Forni over the ablation season 2019.

295

296 Visual inspection of the data showed that at the beginning of the ablation season,  
 297 tardigrade biomass was higher in the lower part of the ablation zone than in the upper part.

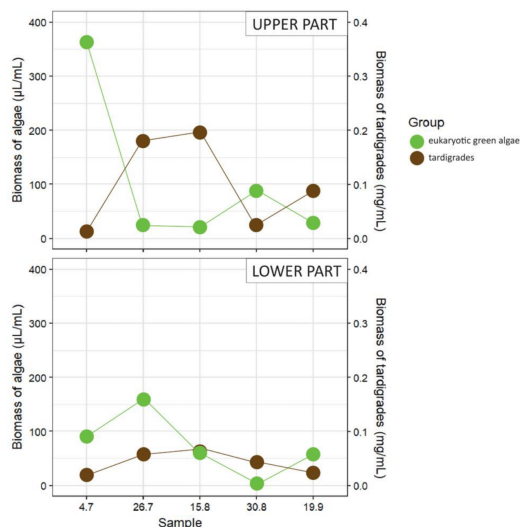


**Figure 2.** Biomass of eukaryotic green algae ( $\mu\text{L}/\text{mL}$ ) and tardigrades ( $\text{mg}/\text{mL}$ ) in the upper and lower part of the Forni Glacier tongue during the ablation season 2019.

From the first timepoint, photoautotrophic biomass in the upper part decreased while that in the lower part increased (Fig. 2).

The biomass of tardigrades in the upper part was significantly related to the

309 biomass of eukaryotic green algae while it did not produce any seasonal trend in the lower part  
 310 (Table 2, Fig. 3).

311 **Table 2.** Linear model of tardigrade biomass on chlorophyta biomass, sampling area and their  
 312 interaction. *P* values were assessed by a randomization method.

Effect	Coef.	Adjusted SE	t	<i>p</i>
Intercept	5.403	2.582	2.093	0.081
log(Chlorophyta biomass)	-0.109	0.239	-0.457	0.601
Upper sampling area	12.602	4.043	3.117	0.013
log(Chlorophyta biomass) * upper sampling area	-1.096	0.371	-2.951	0.018

313

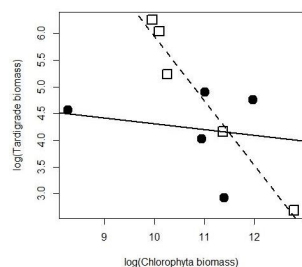
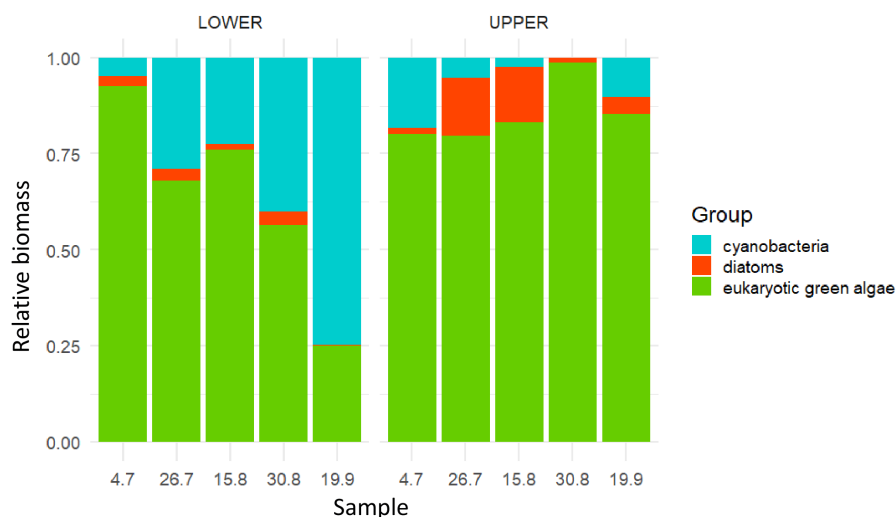


**Figure 3.** Relationship between log-transformed biomass of tardigrades and eukaryotic green algae in the lower (dots and solid line) and upper (squares and dashed line) part of the Forni Glacier ablation zone during the ablation season 2019.

Also, no significant trend in the biomass of tardigrades was found in relation to the biomass of cyanobacteria and diatoms at both parts of the ablation zones (sampling areas) over the

321 season ( $|t_6| \leq 0.543$ , *p* value  $\geq 0.611$ ). On average, the total biomass of tardigrades in the upper  
 322 sampling area did not differ from that of the lower one ( $t_8 = 0.854$ , *p* value = 0.424).

323 The relative biomass of photoautotrophs varied between the upper and lower part of the  
 324 ablation zone (Fig. 4).



325

326 **Figure 4.** Relative biomass of photoautotrophs (cyanobacteria, diatoms, and eukaryotic green  
327 algae) in the upper and lower part of the Forni Glacier tongue during the ablation season 2019.

328

329 RDA analysis of Hellinger transformed biomass of cyanobacteria, diatoms, and  
330 eukaryotic green algae revealed that the community structure of photoautotrophs changed  
331 during the season with different patterns at each part of the ablation zone (sampling date by  
332 area interaction effect:  $F_{1,6} = 6.533$ ,  $p$  value = 0.030 adjusted  $R^2$  of = 0.622, Fig. 5). In the lower  
333 part of the ablation zone, the relative biomass of cyanobacteria significantly increased during  
334 the season ( $|t_6| \leq 4.735$ ,  $P_{FDR} \geq 0.012$ ), the relative biomass of eukaryotic green algae decreased  
335 ( $|t_6| \leq -4.642$ ,  $P_{FDR} \geq 0.012$ ), and diatoms were stable ( $|t_6| \leq -0.238$ ,  $P_{FDR} \geq 0.832$ ). In the upper  
336 part, no taxon showed any significant trend in the relative biomass ( $|t_6| \leq 0.902$ ,  $P_{FDR} \geq 0.764$ ).

337

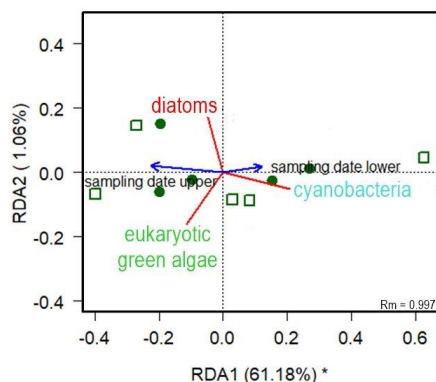
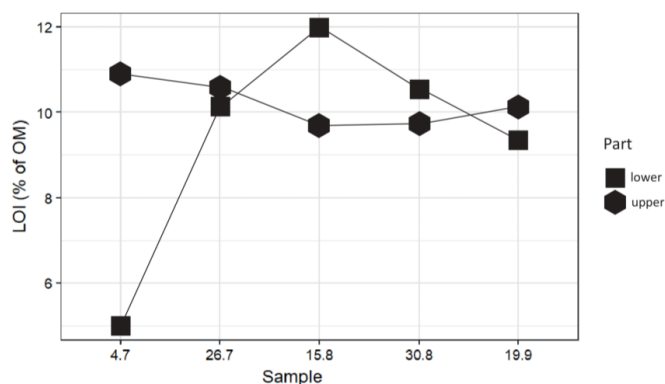


**Figure 5.** RDA correlation triplot of photoautotrophs in the upper (open squares) and the lower (full dots) part of the ablation zone. Blue arrows represent constraining covariates.  $r_M$  is the Mantel correlation coefficient between distance among samples and distance among the point representing them in the plot. Values close to one indicate that the plot accurately represents reciprocal distance among samples.

349

### 350 3.2 Elements and organic matter in cryoconite

351 We observed no significant variation in OM content over the ablation season either at the upper  
352 or the lower part of the ablation zone ( $F_{3,6} = 1.238$ ,  $p$  value = 0.375; Fig. 6).



353

354 **Figure 6.** Percent organic matter content (LOI) in both parts of the ablation zone along the  
355 season.  
356

357 Regarding the general elemental composition, only elements with more than 1000  $\mu\text{g}/\text{kg}$   
358 (Ca, K, P, Si, Al, Mg) were considered. RDA models on standardized elemental abundance  
359 showed that the elemental composition did not vary significantly according to sampling date,  
360 part of the ablation zone, or their interaction ( $F_{3,6} = 0.305$ ,  $p$  value = 0.937). The summary of  
361 data is provided in Table 3 and Figure S1.



362 **Table 3.** The data on biomass of photoautotrophs and consumers, stable isotopic composition  
 363 of cryoconite and consumers, organic matter content (LOI) in cryoconite, and the general  
 364 elemental composition (<1000 µg/kg) of cryoconite on the alpine glacier Forni over the ablation  
 365 season 2019.

Date/Part	Group	4. 7.		26. 7.		15. 8.		30. 8.		19. 9.		
		Lower	Upper	Lower	Upper	Lower	Upper	Lower	Upper	Lower	Upper	
Biomass mm <sup>3</sup> /mL	eukaryotic green algae	89.05	363.46	160.10	24.24	60.97	21.14	3.91	87.31	57.40	28.49	
	cyanobacteria	4.57	83.19	68.21	1.63	18.00	0.64	2.77	0	172.17	3.43	
	diatoms	2.5	7.43	7.37	4.58	1.10	3.63	0.24	1.18	0.92	1.46	
	tardigrades	18.66	13.88	57.29	179.98	63.28	195.41	42.90	24.06	21.86	88.73	
µg/mL												
LOI (%)	cryoconite	5.01	10.88	10.15	10.57	11.97	9.67	10.54	9.74	9.34	10.16	
Stable isotopes (‰)	δ <sup>13</sup> C tardigrades	-25.62	-23.52	-25.89	-27.15	-26.16	-27.23	x	-27.36	-23.96	-26.98	
	δ <sup>15</sup> N tardigrades	x	x	-6.32	-7.22	-7.14	-7.01	x	x	x	-7.34	
	δ <sup>13</sup> C cryoconite		-22.05	-21.29	-21.4	-23.31	-21.42	-23.37	-20.57	-23.46	-20.18	-22.9
			-22.07	-21.25	-21.41	-23.29	-21.70	-23.37	-20.5	-23.35	-20.12	-22.91
			-22.18	-21.2	-21.41	-23.29	-21.73	-23.31	-20.63	-22.3	-20.18	-22.93
			x	x	x	x	x	x	x	x	-20.29	x
	δ <sup>15</sup> N cryoconite		-4.86	-5.18	-5.38	-4.68	-4.96	-4.65	-5.13	-4.66	-4.91	-5.52
			-4.78	-5.15	-5.37	-4.73	-4.93	-4.67	-5.16	-4.61	-4.94	-5.53
			-4.86	-5.29	-5.32	-5.21	-4.94	-4.61	-5.21	-4.64	-4.77	x
	Elements (mg/kg)	Ca	2262.3737	2212.93	3011.6446	3318.53	3131.6666	3127.72	3010.48	2926.14	2580.36	4167.04
K		938.1614	1824.23	1836.3847	2294.27	2489.8232	1854.77	2333.05	1975.69	2051.71	2486.16	
P		1475.1355	4619.07	3477.0035	4435.44	5324.6787	3935.42	4375.48	1298.59	3151.21	4289.11	
Si		1867.8974	3970.48	4848.4904	5700.19	6121.6709	4190.48	6865.62	5159.58	5059.43	7194.23	
Al		3186.3802	8053.97	7904.6442	11113.9	12475.8152	8990.04	11146.5	9121.65	8580.33	8981.54	
Mg		978.7658	2100.21	2158.952	2880.08	3139.3901	2462.2	3106.72	2375.31	2337.62	2311.53	

366

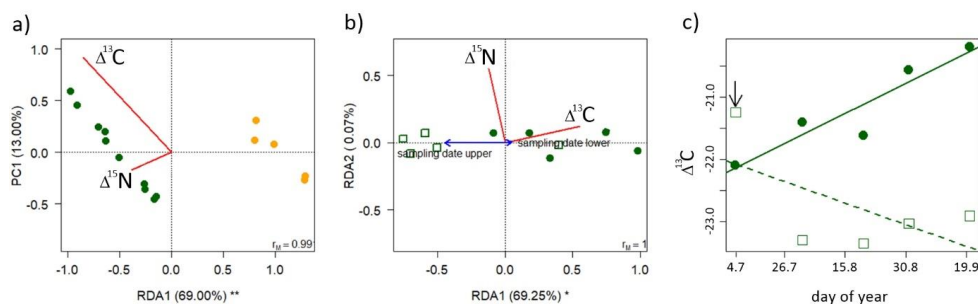
### 367 3.3 Stable isotopic composition of organic matter and consumers

368 An RDA (Fig. 7a) revealed that δ<sup>13</sup>C and δ<sup>15</sup>N of tardigrades significantly differ from isotopic  
 369 values of cryoconite (F<sub>1,15</sub> = 64.755, p value = 0.001, adjusted R<sup>2</sup> = 0.820). Tardigrades were  
 370 depleted in both δ<sup>13</sup>C and δ<sup>15</sup>N (t<sub>13</sub> ≤ -10.968, p value < 0.001) compared to cryoconite. In  
 371 addition, cryoconite and tardigrades appeared to have similarities in fluctuations of their δ<sup>13</sup>C  
 372 values. Further analyses on stable isotopic data of tardigrades were not feasible due to the low  
 373 amount of data for δ<sup>15</sup>N of tardigrades (n ≤ 9), caused by a low number of specimens found in  
 374 samples from some sampling campaigns.

375 A second RDA (Fig. 7b) with parts of the ablation zone, day-of-year, and their interaction  
 376 showed that isotopic values of cryoconite changed along the melting season differently in the  
 377 lower and in the upper sampling area (interaction effect: F<sub>1,6</sub> = 7.786, p value = 0.032, adjusted  
 378 R<sup>2</sup> of the model = 0.693). A linear model calculated for δ<sup>13</sup>C revealed that δ<sup>13</sup>C values were on  
 379 average higher in the lower than in the upper part of the ablation zone (coef. ± SE: 1.592 ±



380 0.389,  $t_6 = 4.095$ ,  $p$  value = 0.010) and changed during the season according to divergent trends  
381 in both parts of the ablation zone (parts of the ablation zone by day-of-year interaction,  $F_{1,6} =$   
382 8.238,  $p$  value = 0.035; Fig. 7c). In particular, the  $\delta^{13}\text{C}$  values increased (were enriched in  $^{13}\text{C}$ )  
383 over the ablation season in the lower part of the ablation zone (coef.  $\pm$  SE:  $0.024 \pm 0.010$ ,  $t_6 =$   
384 2.363,  $p$  value = 0.045) while no relationship was observed for the upper part (coef.  $\pm$  SE: -  
385  $0.017 \pm 0.010$ ,  $t_6 = -1.696$ ,  $p$  value = 0.153), even when the first and most enriched value (Fig.  
386 7c) was removed ( $t_5 = 1.196$ ,  $p$  value = 0.275). No trend for  $\delta^{15}\text{N}$  of OM in cryoconite and  
387 consumers was observed ( $F_{3,6} = 3.150$ ,  $p$  value = 0.108).



388

389 **Figure 7.** RDA correlation triplot of **a)**  $\delta^{13}\text{C}$  and  $\delta^{15}\text{N}$  values in cryoconite (green) and  
390 tardigrades (orange); **b)**  $\delta^{13}\text{C}$  and  $\delta^{15}\text{N}$  values of cryoconite samples collected in the upper (open  
391 squares) and lower (full dots) part of the ablation zone. Blue arrows represent constraining  
392 covariates,  $r_M$  is the Mantel correlation coefficient between distance among samples and  
393 distance among the point representing them in the plot. Values close to one indicate that the  
394 plot accurately represents reciprocal distance among samples; **c)** Scatterplot of  $\delta^{13}\text{C}$  values in  
395 cryoconite in the upper (open squares) and lower (full dots) part of the ablation zone. The black  
396 arrow indicates an influential point whose removal did not change the results.

397  
398

## 399 4. Discussion

### 400 4.1 Photoautotrophs, elemental composition, and organic matter content

401 In our study, the upper part of the ablation zone at the Forni Glacier was dominated by  
402 eukaryotic green algae, whereas, in the lower part, the community structure changed from the  
403 dominance of eukaryotic green algae to a dominance of cyanobacteria during the season.



404 Dominant eukaryotic green algae found within both parts of the ablation zone belonged to  
405 families Mesotaeniaceae and Chlorellaceae, which are common in cryospheric habitats (Di  
406 Bella et al., 2007; Takeuchi et al., 2001b). As discussed by Buda et al. (2020) and Vonnahme  
407 et al. (2016), the fast growth of algae might influence their adaptation to the dynamic conditions  
408 of cryoconite holes on valley glaciers in polar and mountain regions and lead to an increase in  
409 biomass. In Greenland, Svalbard, and the Alps, the temporal or spatial differences in  
410 communities of glacier cyanobacteria and eukaryotic green algae are related to meltwater  
411 availability and physicochemical features of the environment in cryoconite holes (Di Mauro  
412 2020; Stibal et al., 2006; Uetake et al., 2010; Vonnahme et al., 2016). For instance, Stibal et al.  
413 (2012b) observed an increasing abundance of cyanobacteria with increasing nutrient content  
414 and increasing distance from the glacier margin in Greenland. An increase in the proportion of  
415 cyanobacteria at higher elevation of Greenland glaciers was also observed by Uetake et al.  
416 (2010).

417 We did not observe a large variability in general elemental composition between both  
418 parts of the ablation zone in our samples, even though we expected that availability of meltwater  
419 and activity of microorganisms may influence the weathering of mineral grains (e.g. Hoppert  
420 et al., 2004) in holes and consequently release nutrients. However, the lower part of the glacier  
421 tongue was covered by a higher amount of proglacial debris, which could serve as a substrate  
422 to favour the growth of cyanobacteria (Uetake et al., 2016).

423 Even insignificant, seasonal fluctuations and differences in OM content in the upper and  
424 lower part of the ablation zone could indicate that the OM content is spatially dependent and  
425 likely related to the balance between OM produced *in situ* and OM delivered from external  
426 sources. Assuming that the upper part of the glacier tongue is more stable compared to the lower  
427 part, a higher OM content in the upper part follows the experimental results of Buda et al.  
428 (2021), who showed that OM is decomposed faster in dynamic conditions representing at lower



429 elevations. In addition, greater hydrological connectivity and slope of ice tongue may wash up  
430 OM in lower part.

431 It is likely that seasonal patterns in the community structure of photoautotrophs combine  
432 effects of phenology of glacier photoautotrophs, biological control, and physical forces shaping  
433 their community structure. Some photoautotrophs like cyanobacterium *Phormidium* sp. or algae  
434 *Cylindrocystis brebbisoni* dominated along the whole season in our samples. However, for  
435 example cyanobacterium *Pseudanabaena* sp. and *Chroococcus* sp. were present only during  
436 single sampling campaigns, and some like *Trochiscia* sp. occurred during few sampling  
437 campaigns with untraceable presence between them.

#### 438 **4.2 Biomass of photoautotrophs and consumers**

439 The biomass of photoautotrophs and consumers showed different seasonal trends at both parts  
440 of the ablation zone. At the beginning of the ablation season, biomass of all photoautotrophs  
441 decreased with increasing biomass of consumers in the upper part of the glacier, while in the  
442 lower part the biomass of both the consumers and all photoautotrophs increased. At the end of  
443 the season, the biomass of photoautotrophs and consumers showed opposite patterns in both  
444 parts of the ablation zone.

445 On the glacier surface, we cannot exclude physical factors controlling the distribution of  
446 biomass of photoautotrophs and consumers. Based on observations from other Arctic glaciers  
447 (Hodson et al., 2007; Mueller and Pollard, 2004; Zawierucha et al., 2019b), meltwater may be  
448 an important factor in redistribution of cryoconite along the glacier surface. Thus, at the  
449 beginning of the season, meltwater may wash the cryoconite and sediment down from the upper  
450 part of the glacier and cause the input of cryoconite with photoautotrophs to the lower parts as  
451 observed by Takeuchi et al. (2001b).

452 Nevertheless, biological control may be also crucial in cryoconite hole ecosystem  
453 functioning (Cook et al., 2016; McIntyre, 1984). Scheffer et al. (2008) suggested that if



454 densities of consumers are low, algae can escape from top-down control. The observation of  
455 glacier tardigrade *C. klebelsbergi* under laboratory conditions revealed that this species actively  
456 feeds on a mix of *Chlorella* and *Chlorococcum* both belonging to Chlorophyta (K. Zawierucha  
457 pers. observ.). Moreover, Zawierucha et al. (2022) showed that in the field *C. klebelsbergi* feed  
458 on the eukaryotic green algae (Trebouxiophyceae).

459 We observed a negative relation between the biomass of eukaryotic green algae and the  
460 biomass of tardigrades in the upper part of the glacier tongue. In the same part, the only  
461 sampling date with reduced biomass of tardigrades accompanied with an increase in the  
462 biomass of eukaryotic green algae was affected by the presence of numerous small tardigrade  
463 juveniles (K. Zawierucha pers. observ.) likely decreasing the overall biomass of consumers and  
464 potentially favour the growth of algae. Indeed, Vonnahme et al. (2016) suggested that  
465 microalgae in cryoconite holes can increase their densities (cell size, formation of colonies) as  
466 a response to the grazing pressure.

467 On the contrary, the biomass of photoautotrophs in the lower part of the ablation area  
468 seemed to be affected by temporal or episodic changes more than consumers, which remained  
469 almost stable with a slight increase in their biomass at the beginning of the season and a slight  
470 decrease at the end. Although, Scheffer et al. (2008) suggested that if organisms are slow-  
471 growing, they are much less affected by episodic pulses (e.g. mirroring the lower part of the  
472 ablation zone), the biomass in the lower part, of both algae and grazers, didn't build up so fast  
473 as in the upper part, most probably due to less of stability. However, our assumptions are based  
474 on observation from one season only and require additional testing in the future.

#### 475 **4.3 $\delta^{13}\text{C}$ and $\delta^{15}\text{N}$ isotopic composition**

476 Changes in irradiation, higher photosynthetic activity, higher growth rate or differences in the  
477 nutrient pool could change the proportion of carbon and nitrogen forms in the cryoconite and  
478 consequently affect the isotopic values of the biota (e.g. Beardall et al., 1982; Gu et al., 2006;



479 Lehmann et al., 2004; Senese et al., 2016; Schmidt et al., 2022; Yoshii et al., 1999). The more  
480 depleted  $\delta^{13}\text{C}$  and  $\delta^{15}\text{N}$  of tardigrades compared to the cryoconite organic matter on the Forni  
481 Glacier corroborates the results from Arctic cryoconite holes (Novotná Jaroměřská et al., 2021)  
482 and microbial mats in Antarctica (Almela et al., 2019; Velázquez et al., 2017). However, since  
483 microbial mats are different systems, organic matter in cryoconite holes on the Forni Glacier  
484 was depleted in heavy carbon ( $^{13}\text{C}$ ) and nitrogen ( $^{15}\text{N}$ ) isotopes and the differences between  
485  $\delta^{13}\text{C}$  and  $\delta^{15}\text{N}$  of organic matter and consumers were higher. Based on previous models (Almela  
486 et al., 2019; Velázquez et al., 2017), tardigrades likely fed on cyanobacteria, diatoms, and POM  
487 (particulate organic matter)  $< 30 \mu\text{m}$ . Even though cryoconite from the Forni Glacier contains  
488 consumable cyanobacteria and algae, our results do not correspond with the standard  
489 fractionation between consumer and food (DeNiro and Epstein, 1978; Yoshii et al., 1999).

490         Since tardigrades in all samples followed fluctuations of  $\delta^{13}\text{C}$  values of cryoconite, we  
491 suggest that some components of cryoconite serve indeed as their food source (Novotná  
492 Jaroměřská et al., 2021). Nevertheless, our results are probably highly influenced by the stable  
493 isotopic composition of the unconsumed part of cryoconite, which increases the differences  
494 between food and consumers.

495         Despite the significance of autochthonous production of microbes, most of the organic  
496 matter in cryoconite holes seems to be of allochthonous origin (Stibal et al., 2008). Forni is a  
497 relatively small glacier and the allochthonous material covers the whole ablation zone with its  
498 inorganic part predominantly originated from surrounding rocks (Azzoni et al., 2016).  
499 Therefore, the low  $\delta^{13}\text{C}$  of OM in cryoconite from the Forni Glacier compared to cryoconite  
500 from Antarctic glaciers with higher occurrence of photosynthetically active cyanobacteria  
501 (Schmidt et al., 2022) or microbial mats (Almela et al., 2019; Velázquez et al., 2017) may be  
502 influenced by the prevailing allochthonous organic matter which can lower the  $\delta^{13}\text{C}$  compared  
503 to material formed *in situ* (Musilova et al., 2015; Pautler et al., 2013; Stibal et al., 2008).



504           The differences in  $\delta^{13}\text{C}$  of OM in cryoconite between parts of the ablation zone and the  
505 increasing seasonal trend in  $\delta^{13}\text{C}$  in the lower part of the glacier tongue can be the result of the  
506 seasonal evolution in microbial community structure and the dominance of *in situ* microbial  
507 production predominantly using isotopically heavy DIC (dissolved inorganic carbon) instead  
508 of atmospheric  $\text{CO}_2$  (Musilova et al., 2015; Stibal and Tranter, 2007). Communities of  
509 eukaryotic green algae were dominated by Chlorellales and Zygnematales in both parts of the  
510 ablation zone. Based on Beardall et al. (1982), nitrogen limitation in *Chlorella emersonii* results  
511 in higher  $\delta^{13}\text{C}$  values due to the higher accumulation of  $\text{CO}_2$  and lower fractionation against  
512  $^{13}\text{C}$  by RuBiSCO (ribulose 1,5 bisphosphate carboxylase-oxygenase). The  $\delta^{15}\text{N}$  ratios were not  
513 different in cryoconite between both parts of the ablation zone. Also, we were unable to analyse  
514 the isotopic composition of each group of photoautotrophs separately, so we could not reveal  
515 their contribution to the overall isotopic signal of OM in cryoconite.

## 516 **5. Conclusions**

517 In this study, we described spatial changes in the community structure, biomass, and stable  
518 carbon and nitrogen isotopic composition of biota from cryoconite holes in the ablation tongue  
519 of the alpine glacier Forni during the summer season. Since we did not observe any significant  
520 fluctuations in the general elemental composition of cryoconite, changes in the composition  
521 and biomass of photoautotrophs and consumers in both parts of the ablation zone indicated  
522 phenological or ecological controls over their communities. Some photoautotrophs appeared  
523 only during specific sampling days pointing out that rare species might be overlooked during  
524 single sampling campaigns. Based on our data we assume that photoautotrophs in cryoconite  
525 holes might be controlled by grazing; they may increase their biomass as a protection against  
526 overgrazing or escape from top-down control. However, other factors such as influence of  
527 meltwater, weathering, or the input of matter from adjacent sources cannot be overlooked and  
528 require further investigation in studies on seasonal development of cryoconite community in



529 the future. Seasonal increase in  $\delta^{13}\text{C}$  in the lower part of the glacier tongue may suggest  
530 potential changes in the microbial community structure, nutrient concentration, or differences  
531 in the source of OM. We demonstrated that the recognition of the community structure of  
532 cryoconite holes requires a broad-scale and seasonal approach since biological communities  
533 vary in time and space on the glacier surface.

534 **Data availability.** All data are available upon request to TNJ and KZ.

535 **Author contributions.** TNJ performed research, analyzed data, and wrote the paper. RA  
536 analyzed data and wrote the paper. DR, MP, PN, JS-K and PK performed research and analyzed  
537 data. AF and FP performed research. LV analyzed data. TK performed research and analyzed  
538 data. KZ conceived and designed study, performed research, analyzed data, and wrote the paper.

539 All authors contributed significantly to the redaction of the paper.

540 **Competing interests.** The authors declare that they have no conflict of interest.

541 **Acknowledgments.** We would like to thank Sabina Sikorska, Aleksandra Kozłowska and  
542 Masato Ono for their help in biomass measurement and their support in preparation of  
543 supplementary figures.

544 **Financial support.** This research (analyses on organic matter, biomass measurements, the  
545 investigation of food preference and biotic control) was supported by the grant OPUS funded  
546 by National Science Centre (no. 2018/31/B/NZ8/00198) awarded to KZ. Analyses of stable  
547 isotopic composition were supported by a Charles University research grant GA UK (Charles  
548 University Grant Agency), grant no. 596120 awarded to TNJ.

549

550

551



552 **References**

- 553 Almela, P., Velázquez, D., Rico, E., Justel, A., and Quesada, A.: Carbon pathways through the  
554 food web of a microbial mat from Byers Peninsula, Antarctica, *Front. Microbiol.*, 10, 628,  
555 <https://doi.org/10.3389/fmicb.2019.00628>, 2019.
- 556 Anesio, A. M. and Laybourn-Parry, J.: Glaciers and ice sheets as a biome, *Trends Ecol.*  
557 *Evol.*, 27, 219–225, <https://doi.org/10.1016/j.tree.2011.09.012>, 2012.
- 558 Azzoni, R. S., Senese, A., Zerboni, A., Maugeri, M., Smiraglia, C., and Diolaiuti, G. A.:  
559 Estimating ice albedo from fine debris cover quantified by a semi-automatic method: the case  
560 study of Forni Glacier, Italian Alps, *The Cryosphere*, 10, 665–679, [https://doi.org/10.5194/tc-](https://doi.org/10.5194/tc-10-665-2016)  
561 [10-665-2016](https://doi.org/10.5194/tc-10-665-2016), 2016.
- 562 Bagshaw, E. A., Tranter, M., Fountain, A. G., Welch, K., Basagic, H. J., and Lyons, W. B.: Do  
563 cryoconite holes have the potential to be significant sources of C, N, and P to downstream  
564 depauperate ecosystems of Taylor Valley, Antarctica? *Arct. Antarct. Alp. Res.*, 45, 440–454,  
565 <https://doi.org/10.1657/1938-4246-45.4.440>, 2013.
- 566 Beardall, J., Griffiths, H., and Raven, J. A.: Carbon isotope discrimination and the CO<sub>2</sub>  
567 accumulating mechanism in *Chlorella emersonii*, *J. Exp. Bot.*, 33, 729–737,  
568 <https://doi.org/10.1093/jxb/33.4.729>, 1982.
- 569 Brodie, C. R., Leng, M. J., Casford, J. S., Kendrick, C. P., Lloyd, J. M., Yongqiang, Z., and  
570 Bird, M. I.: Evidence for bias in C and N concentrations and <sup>13</sup>C composition of terrestrial and  
571 aquatic organic materials due to preanalysis acid preparation methods, *Chem. Geol.*, 282,  
572 67–83, <https://doi.org/10.1016/j.chemgeo.2011.01.007>, 2011.
- 573 Buda, J., Łokas, E., Pietryka, M., Richter, D., Magowski, W., Iakovenko, N., Porazinska, D.,  
574 Budzik, T., Grabiec, M., Grzesiak, J., Klimaszyk, P., Gaca, P., and Zawierucha, K.: Biotope



- 575 and biocenosis of cryoconite hole ecosystems on ecology glacier in the maritime Antarctic, *Sci.*  
576 *Total Environ.*, 724, 138112, <https://doi.org/10.1016/j.scitotenv.2020.138112>, 2020.
- 577 Buda, J., Poniecka, E. A., Rozwalak, P., Ambrosini, R., Bagshaw, E. A., Franzetti, A.,  
578 Klimaszyk, P., Nawrot, A., Pietryka, M., Richter, D., and Zawierucha, K.: Is oxygenation  
579 related to the decomposition of organic matter in cryoconite holes? *Ecosystems*, 1–12,  
580 <https://doi.org/10.1007/s10021-021-00729-2>, 2021.
- 581 Cameron, K. A., Hodson, A. J., and Osborn, M.: Carbon and nitrogen biogeochemical cycling  
582 potentials of supraglacial cryoconite communities, *Polar Biol.*, 35, 1375–1393,  
583 <https://doi.org/10.1007/s00300-012-1178-3>, 2012.
- 584 Citterio, M., Diolaiuti, G., Smiraglia, C., Verza, G. P., and Meraldi, E.: Initial results from the  
585 Automatic Weather Station (AWS) on the ablation tongue of Forni Glacier (Upper Valtellina,  
586 Italy), *Geogr. Fis. e Din. Quat.*, 30, 141–151, 2007.
- 587 Coesel, P. F. and Meesters, K. J.: *Mesotaeniaceae and Desmidiaceae of the European Lowlands.*  
588 *Desmids of the Lowlands*, KNNV Publishing, Leiden, Netherlands, 351 pp., 2007.
- 589 Colombo, N., Bocchiola, D., Martin, M., Confortola, G., Salerno, F., Godone, D., D’Amico,  
590 M. E., and Freppaz, M.: High export of nitrogen and dissolved organic carbon from an Alpine  
591 glacier (Indren Glacier, NW Italian Alps), *Aquat. Sci.*, 81, 1–13,  
592 <https://doi.org/10.1007/s00027-019-0670-z>, 2019.
- 593 Cook, J., Edwards, A., Takeuchi, N., and Irvine-Fynn, T.: Cryoconite: The dark biological  
594 secret of the cryosphere, *PPG: Earth and Environment*, 40, 66–111,  
595 <https://doi.org/10.1177/0309133315616574>, 2016.
- 596 Dastyh, H., Kraus, J., and Thaler, K.: Redescription and notes on the biology of the glacier  
597 tardigrade *Hypsibius klebelsbergi* Mihelcic, 1959 (Tardigrada), based on material from Ötztal



- 598 Alps, Austria, Mitteilungen aus dem Hamburgischen Zoologischen Museum und Institut, 100,  
599 77–100, 2003.
- 600 DeNiro, M. J. and Epstein, S.: Influence of diet on the distribution of carbon isotopes in animals,  
601 Geochim. Cosmochim. Ac., 42, 495–506, [https://doi.org/10.1016/0016-7037\(78\)90199-0](https://doi.org/10.1016/0016-7037(78)90199-0),  
602 1978.
- 603 Di Bella, M., La Rocca, N., Moro, I., Andreoli, C., Baldan, B., and Rascio, N.: Respiratory  
604 activity of the cryophilic alga “*Chlorella*” *saccharophila* at different temperatures, Caryologia,  
605 60, 111–114, <https://doi.org/10.1080/00087114.2007.10589556>, 2007.
- 606 Di Mauro, B., Garzonio, R., Baccolo, G., Franzetti, A., Pittino, F., Leoni, B., Remias, D.,  
607 Colombo, R., and Rossini, M.: Glacier algae foster ice-albedo feedback in the European  
608 Alps, Sci. Rep., 10, 1–9, <https://doi.org/10.1038/s41598-020-61762-0>, 2020.
- 609 Edwards, A., Rassner, S. M. E., Anesio, A. M., Worgan, H. J., Irvine-Fynn, T. D. L., Williams,  
610 H. W., Sattler, B., and Griffith, G. W.: Contrasts between the cryoconite and ice-marginal  
611 bacterial communities of Svalbard glaciers, Polar Res., 32, 19468,  
612 <https://doi.org/10.3402/polar.v32i0.19468>, 2013.
- 613 Fountain, A. G., Tranter, M., Nylen, T. H., Lewis, K. J., and Mueller, D. R.: Evolution of  
614 cryoconite holes and their contribution to meltwater runoff from glaciers in the McMurdo Dry  
615 Valleys, Antarctica, J. Glaciol., 50, 35–45, doi:10.3189/172756504781830312, 2004.
- 616 Franzetti, A., Navarra, F., Tagliaferri, I., Gandolfi, I., Bestetti, G., Minora, U., Azzoni, R. S.,  
617 Diolaiuti, G., Smiraglia, C., and Ambrosini, R.: Potential sources of bacteria colonizing the  
618 cryoconite of an Alpine glacier, PLoS One, 12, e0174786,  
619 <https://doi.org/10.1371/journal.pone.0174786>, 2017.



- 620 Gobbi, M., Ambrosini, R., Casarotto, C., Diolaiuti, G., Ficetola, G. F., Lencioni, V., Seppi, R.,  
621 Smiraglia, C., Tampucci, D., Valle, B., and Caccianiga, M.: Vanishing permanent glaciers:  
622 climate change is threatening a European Union habitat (Code 8340) and its poorly known  
623 biodiversity, *Biodivers. Conserv.*, 30, 2267–2276, [https://doi.org/10.1007/s10531-021-02185-](https://doi.org/10.1007/s10531-021-02185-9)  
624 9, 2021.
- 625 Gu, B., Chapman, A. D., and Schelske, C. L.: Factors controlling seasonal variations in stable  
626 isotope composition of particulate organic matter in a softwater eutrophic lake, *Limnol.*  
627 *Oceanogr.*, 51, 2837–2848, <https://doi.org/10.4319/lo.2006.51.6.2837>, 2006.
- 628 Hallas, T. E. and Yeates, G. W.: Tardigrada of the soil and litter of a Danish beech forest,  
629 *Pedobiologia*, 12, 287–304, 1972.
- 630 Hindak, F.: Key to the unbranched filamentous green algae (Ulotrichineae, Ulotrichales,  
631 Chlorophyceae), *Bulletin Slovenskej botanickej spoločnosti pri SAV*, Bratislava, Slovakia, 77  
632 pp., 1996.
- 633 Hodson, A., Anesio, A. M., Ng, F., Watson, R., Quirk, J., Irvine-Fynn, T., Dye, A., Clark, Ch.,  
634 McCloy, P., Kohler, P., and Sattler, B.: A glacier respire: Quantifying the distribution and  
635 respiration CO<sub>2</sub> flux of cryoconite across an entire Arctic supraglacial ecosystem, *J. Geophys.*  
636 *Res.*, 112, G04S36, <https://doi.org/10.1029/2007JG000452>, 2007.
- 637 Hoppert, M., Flies, C., Pohl, W., Günzl, B., and Schneider, J.: Colonization strategies of  
638 lithobiontic microorganisms on carbonate rocks, *Environ. Geol.*, 46, 421–428,  
639 <https://doi.org/10.1007/s00254-004-1043-y>, 2004.
- 640 Hutorowicz, A.: Opracowanie standardowych objętości komórek do szacowania biomasy  
641 wybranych taksonów glonów planktonowych wraz z określeniem sposobu pomiarów I  
642 szacowania [Development of standard cell volume estimation for planktonic algae  
643 biomass determination], GIOŚ, Olsztyn, Poland, 1–40 pp., 2006 (in Polish).



- 644 John, D. M. and Rindi, F.: Filamentous (Nonconjugating) and Plantlike Green Algae. Wehr, J.  
645 D., Sheath, R. G., Kociolek, J. P. (Eds.): Freshwater algae of North America: Ecology and  
646 classification, Academic, San Diego, U. S., 375–427 pp., 2015.
- 647 Komárek, J. and Anagnostidis, K.: Cyanoprokaryota. 2. Teil: Oscillatoriales. Büdel, B.,  
648 Gärtner, G., Krienitz, L., Schagerl, M. (Eds.): Süßwasserflora von Mitteleuropa, Bd. 19 (2),  
649 Elsevier GmbH, München, Germany, 1–759 pp., 2005.
- 650 Krammer, K. and Lange-Bertalot, H.: Bacillariophyceae 1. Naviculaceae. Süßwasserflora von  
651 Mitteleuropa, Gustav Fischer Verlag, Stuttgart, Germany, 1–876 pp., 1986.
- 652 Krammer, K. and Lange-Bertalot, H.: Bacillariophyceae 2/3. Centrales, Fragilariaceae,  
653 Eunotiaceae. Ettl, H., Gerloff, J., Heynig, H., Mollenhauer, D. (Eds.), Süßwasserflora von  
654 Mitteleuropa, Gustav Fischer, Stuttgart, Germany, 1–576 pp., 1991a.
- 655 Krammer, K. and Lange-Bertalot, H.: Bacillariophyceae 4. Achnantheaceae, Kritische  
656 Ergänzungen zu *Navicula* (Lineolatae), *Gomphonema* Gesamtliteraturverzeichnis Teil 1–4.  
657 Ettl, H., Gärtner, G., Gerloff, J., Heynig, H., Mollenhauer, D. (Eds.), Süßwasserflora von  
658 Mitteleuropa 2, Spektrum Akademischer Verlag, Heidelberg, Germany, 1–468 pp., 1991b.
- 659 Lehmann, M. F., Bernasconi, S. M., McKenzie, J. A., Barbieri, A., Simona, M., and Veronesi,  
660 M.: Seasonal variation of the  $\delta^{13}\text{C}$  and  $\delta^{15}\text{N}$  of particulate and dissolved carbon and nitrogen in  
661 Lake Lugano: Constraints on biogeochemical cycling in a eutrophic lake, *Limnol.*  
662 *Oceanogr.*, 49, 415–429, <https://doi.org/10.4319/lo.2004.49.2.0415>, 2004.
- 663 MacDonell, S. and Fitzsimons, S.: The formation and hydrological significance of cryoconite  
664 holes, *PPG: Earth and Environment*, 32, 595–610, <https://doi.org/10.1177/0309133308101382>,  
665 2008.



- 666 McIntyre, N. F.: Cryoconite hole thermodynamics, *Can. J. Earth Sci.*, 21, 152–156,  
667 <https://doi.org/10.1139/e84-016>, 1984.
- 668 Mihelcic, F.: Zwei neue Tardigraden aus der Gattung *Hypsibills* THULIN aus Osttirol  
669 (Osterreich), Systematisches zur Gattung *Hypsibills* THULIN, *Zool. Anz.*, 163, 254–261, 1959.
- 670 Mueller, D. R. and Pollard, W. H.: Gradient analysis of cryoconite ecosystems from two polar  
671 glaciers, *Polar Biol.*, 27, 66–74, <https://doi.org/10.1007/s00300-003-0580-2>, 2004.
- 672 Musilova, M., Tranter, M., Bennett, S. A., Wadham, J., and Anesio, A. M.: Stable microbial  
673 community composition on the Greenland Ice Sheet, *Front. Microbiol.*, 6, 193,  
674 <https://doi.org/10.3389/fmicb.2015.00193>, 2015.
- 675 Novotná Jaroměřská, T., Trubač, J., Zawierucha, K., Vondrovicová, L., Devetter, M., and  
676 Žárský, J. D.: Stable isotopic composition of top consumers in Arctic cryoconite holes:  
677 revealing divergent roles in a supraglacial trophic network, *Biogeosciences*, 18, 1543–1557,  
678 <https://doi.org/10.5194/bg-18-1543-2021>, 2021.
- 679 Pautler, B. G., Dubnick, A., Sharp, M. J., Simpson, A. J., and Simpson, M. J.: Comparison of  
680 cryoconite organic matter composition from Arctic and Antarctic glaciers at the molecular-  
681 level, *Geochim. Cosmochim. Acta*, 104, 1–18, <https://doi.org/10.1016/j.gca.2012.11.029>,  
682 2013.
- 683 Pittino, F., Maglio, M., Gandolfi, I., Azzoni, R., Diolaiuti, G., Ambrosini, R., and Franzetti, A.:  
684 Bacterial communities of cryoconite holes of a temperate alpine glacier show both seasonal  
685 trends and year-to-year variability, *Ann. Glaciol.*, 59, 1–9, doi:10.1017/aog.2018.16, 2018.
- 686 Poniecka, E. A., Bagshaw, E. A., Sass, H., Segar, A., Webster, G., Williamson, C., Anesio, A.  
687 M., and Tranter, M.: Physiological capabilities of cryoconite hole microorganisms, *Front.*  
688 *Microbiol.*, 11, 1783, <https://doi.org/10.3389/fmicb.2020.01783>, 2020.



- 689 Post, E. and Stenseth, N. C.: Climatic variability, plant phenology, and northern ungulates,  
690 Ecology, 80, 1322–1339, [https://doi.org/10.1890/0012-](https://doi.org/10.1890/0012-9658(1999)080[1322:CVPPAN]2.0.CO;2)  
691 9658(1999)080[1322:CVPPAN]2.0.CO;2, 1999.
- 692 Rozwalak, P., Podkowa, P., Buda, J., Niedzielski, P., Kawecki, S., Ambrosini, R., Azzoni, R.  
693 S., Baccolo, G., Ceballos, J. L., Cook, J., Di Mauro, B., Ficetola, G. F., Franzetti, A., Ignatiuk,  
694 D., Klimaszuk, P., Łokas, E., Ono, M., Parnikoza, I., Pietryka, M., Pittino, F., Poniecka, E.,  
695 Porazinska, D. L., Richter, D., Schmidt, S. K., Sommers, P., Souza-Kasprzyk, J., Stibal, M.,  
696 Szczuciński, W., Uetake, J., Wejnerowski, Ł., Yde, J. C., Takeuchi, N., and Zawierucha, K.:  
697 Cryoconite – From minerals and organic matter to bioengineered sediments on glacier's  
698 surfaces, *Sci. Total Environ.*, 807, 150874, <https://doi.org/10.1016/j.scitotenv.2021.150874>,  
699 2022.
- 700 Scheffer, M., Van Nes, E. H., Holmgren, M., and Hughes, T.: Pulse-driven loss of top-down  
701 control: the critical-rate hypothesis, *Ecosystems*, 11, 226–237,  
702 <https://doi.org/10.1016/j.scitotenv.2021.150874>, 2008.
- 703 Schmidt, S. K., Johnson, B. W., Solon, A. J., Sommers, P., Darcy, J. L., Vincent, K., Vimercati,  
704 L., Fountain, A. G., and Porazinska, D. L.: Microbial biogeochemistry and phosphorus  
705 limitation in cryoconite holes on glaciers across the Taylor Valley, McMurdo Dry Valleys,  
706 Antarctica, *Biogeochemistry*, 158, 313–326, <https://doi.org/10.1007/s10533-022-00900-4>,  
707 2022.
- 708 Senese, A., Diolaiuti, G., Mihalcea, C., and Smiraglia, C.: Energy and Mass Balance of Forni  
709 Glacier (Stelvio National Park, Italian Alps) from a Four-year Meteorological Data Record,  
710 *Arct. Antarct. Alp. Res.*, 44, 122–134, <https://doi.org/10.1657/1938-4246-44.1.122>, 2012.
- 711 Senese, A., Maugeri, M., Ferrari, S., Confortola, G., Soncini, A., Bocchiola, D., and Diolaiuti,  
712 G.: Modelling shortwave and longwave downward radiation and air temperature driving



713 ablation at the Forni Glacier (Stelvio National Park, Italy), *Geografia Fisica e Geomorfologia*,  
714 39, 89–100, <https://dx.doi.org/10.4461/GFDQ.2016.39.9>, 2016.

715 Senese, A., Maugeri, M., Meraldi, E., Verza, G. P., Azzoni, R. S., Compostella, C., and  
716 Diolaiuti, G.: Estimating the snow water equivalent on a glacierized high elevation site (Forni  
717 Glacier, Italy), *The Cryosphere*, 12, 1293–1306, <https://doi.org/10.5194/tc-12-1293-2018>,  
718 2018.

719 Senese, A., Manara, V., Maugeri, M., and Diolaiuti, G. A.: Comparing Measured Incoming  
720 Shortwave and Longwave Radiation on a Glacier Surface with Estimated Records from Satellite  
721 and Off-Glacier Observations: A Case Study for the Forni Glacier, Italy, *Remote Sens.*, 12,  
722 3719, <https://doi.org/10.3390/rs12223719>, 2020.

723 Shain, D. H., Novis, P. M., Cridge, A. G., Zawierucha, K., Geneva, A. J., and Dearden, P. K.:  
724 Five animal phyla in glacier ice reveal unprecedented biodiversity in New Zealand's Southern  
725 Alps, *Sci. Rep.*, 11, 3898, <https://doi.org/10.1038/s41598-021-83256-3>, 2021.

726 Shaw, E. A., Adams, B. J., Barrett, J. E., Lyons, W. B., Virginia, R. A., and Wall, D. H.: Stable  
727 C and N isotope ratios reveal soil food web structure and identify the nematode *Eudorylaimus*  
728 *antarcticus* as an omnivore–predator in Taylor Valley, Antarctica, *Polar Biol.*, 41, 1013–1018,  
729 <https://doi.org/10.1007/s00300-017-2243-8>, 2018.

730 Sommers, P., Porazinska, D. L., Darcy, J. L., Zamora, F., Fountain, A. G., and Schmidt, S. K.:  
731 Experimental cryoconite holes as mesocosms for studying community ecology, *Polar Biol.*, 42,  
732 1973–1984, <https://doi.org/10.1007/s00300-019-02572-7>, 2019.

733 Stibal, M., Šabacká, M., and Kaštovská, K.: Microbial communities on glacier surfaces in  
734 Svalbard: impact of physical and chemical properties on abundance and structure of  
735 cyanobacteria and algae, *Microb. Ecol.*, 52, 644–654, [https://doi.org/10.1007/s00248-006-](https://doi.org/10.1007/s00248-006-9083-3)  
736 9083-3, 2006.



- 737 Stibal, M. and Tranter, M.: Laboratory investigation of inorganic carbon uptake by cryoconite  
738 debris from Werenskioldbreen, Svalbard, J. Geophys. Res. Biogeosci., 112, G4,  
739 <https://doi.org/10.1029/2007JG000429>, 2007.
- 740 Stibal, M., Tranter, M., Benning, L. G., and Řehák, J.: Microbial primary production on an  
741 Arctic glacier is insignificant in comparison with allochthonous organic carbon input, Environ.  
742 Microbiol., 10, 2172–2178, <https://doi.org/10.1111/j.1462-2920.2008.01620.x>, 2008.
- 743 Stibal, M., Šabacká, M., and Žárský, J.: Biological processes on glacier and ice sheet surfaces,  
744 Nat. Geosci., 5, 771, <https://doi.org/10.1038/ngeo1611>, 2012a.
- 745 Stibal, M., Telling, J., Cook, J., Mak, K. M., Hodson, A., and Anesio, A. M.: Environmental  
746 controls on microbial abundance and activity on the Greenland ice sheet: a multivariate analysis  
747 approach, Microbial Ecol., 63, 74–84, <https://doi.org/10.1007/s00248-011-9935-3>, 2012b.
- 748 Takeuchi, N., Kohshima, S., and Seko, K.: Structure, formation, and darkening process of  
749 albedo-reducing material (cryoconite) on a Himalayan glacier: a granular algal mat growing on  
750 the glacier, Arct. Antarct. Alp. Res., 33, 115–122,  
751 <https://doi.org/10.1080/15230430.2001.12003413>, 2001a.
- 752 Takeuchi, N.: The altitudinal distribution of snow algae on an Alaska glacier (Gulkana Glacier  
753 in the Alaska Range), Hydrol. Process., 15, 3447–3459, <https://doi.org/10.1002/hyp.1040>,  
754 2001b.
- 755 Takeuchi, N.: Seasonal and altitudinal variations in snow algal communities on an Alaskan  
756 glacier (Gulkana glacier in the Alaska range), Environ. Res. Lett., 8, 035002,  
757 <https://doi.org/10.1088/1748-9326/8/3/035002>, 2013.



- 758 Uetake, J., Naganuma, T., Hebsgaard, M. B., Kanda, H., and Kohshima, S.: Communities of  
759 algae and cyanobacteria on glaciers in west Greenland, *Polar Sci.*, 4, 71–80,  
760 <https://doi.org/10.1016/j.polar.2010.03.002>, 2010.
- 761 Uetake, J., Tanaka, S., Segawa, T., Takeuchi, N., Nagatsuka, N., Motoyama, H., and Aoki, T.:  
762 Microbial community variation in cryoconite granules on Qaanaaq Glacier, NW  
763 Greenland, *FEMS Microbiol. Ecol.*, 92, fiw127, <https://doi.org/10.1093/femsec/fiw127>, 2016.
- 764 Vecchi, M., Kossi Adakpo, L., Dunn, R. R., Nichols, L. M., Penick, C. A., Sanders, N. J.,  
765 Rebecchi, L., and Guidetti, R.: The toughest animals of the Earth versus global warming:  
766 Effects of long-term experimental warming on tardigrade community structure of a temperate  
767 deciduous forest, *Ecol. Evol.*, 11, 9856–9863, <https://doi.org/10.1002/ece3.7816>, 2021.
- 768 Velázquez, D., Jungblut, A. D., Rochera, C., Rico, E., Camacho, A., and Quesada, A.: Trophic  
769 interactions in microbial mats on Byers Peninsula, maritime Antarctica, *Polar Biol.*, 40, 1115–  
770 1126, <https://doi.org/10.1007/s00300-016-2039-2>, 2017.
- 771 Vindušková, O., Jandová, K., and Frouz, J.: Improved method for removing siderite by in situ  
772 acidification before elemental and isotope analysis of soil organic carbon, *J. Plant Nutr. Soil*  
773 *Sc.*, 182, 82–91, <https://doi.org/10.1002/jpln.201800164>, 2019.
- 774 Vonnahme, T. R., Devetter, M., Žárský, J. D., Šabacká, M., and Elster, J.: Controls on  
775 microalgal community structures in cryoconite holes upon high-Arctic glaciers, Svalbard,  
776 *Biogeosciences*, 13, 659–674, <https://doi.org/10.5194/bg-13-659-2016>, 2016.
- 777 Walther, G. R., Post, E., Convey, P., Menzel, A., Parmesan, C., Beebee, T. J., Fromentin, J.-  
778 M., Hoegh-Guldberg, O., and Bairlein, F.: Ecological responses to recent climate  
779 change, *Nature*, 416, 389–395, <https://doi.org/10.1038/416389a>, 2002.



- 780 Wang, Q., Li, Y., and Wang, Y.: Optimizing the weight loss-on-ignition methodology to  
781 quantify organic and carbonate carbon of sediments from diverse sources, *Environ. Monit.*  
782 *Assess.*, 174, 241–257, <https://doi.org/10.1007/s10661-010-1454-z>, 2011.
- 783 Wharton, R. A., McKay, Ch. P., Simmons, G. M., and Parker, B. C.: Cryoconite holes on  
784 glaciers, *Bioscience*, 35, 499–503, <https://doi.org/10.2307/1309818>, 1985.
- 785 Williamson, C. J., Cook, J., Tedstone, A., Yallop, M., McCutcheon, J., Poniecka, E., Campbell,  
786 D., Irvine-Fynn, T., McQuaid, J., Tranter, M., Perkins, R., and Anesio, A.: Algal  
787 photophysiology drives darkening and melt of the Greenland Ice Sheet, *Proc. Natl. Acad. Sci.*  
788 *U.S.A.*, 117, 5694–5705, <https://doi.org/10.1073/pnas.1918412117>, 2020.
- 789 Winkel, M., Trivedi, C. B., Mourot, R., Bradley, J. A., Vieth-Hillebrand, A., and Benning, L.  
790 G.: Seasonality of Glacial Snow and Ice Microbial Communities, *Front. Microbiol.*, 13,  
791 876848, <https://doi.org/10.3389/fmicb.2022.876848>, 2022.
- 792 Yallop, M. L., Anesio, A. M., Perkins, R. G., Cook, J., Telling, J., Fagan, D., MacFarlane, J.,  
793 Stibal, M., Barker, G., Bellas, Ch., Hodson, A., Tranter, M., Wadham, J., and Roberts, N. W.:  
794 Photophysiology and albedo-changing potential of the ice algal community on the surface of  
795 the Greenland ice sheet, *ISME J.*, 6, 2302–2313, <https://doi.org/10.1038/ismej.2012.107>, 2012.
- 796 Yoshii, K., Melnik, N. G., Timoshkin, O. A., Bondarenko, N. A., Anoshko, P. N., Yoshioka,  
797 T., and Wada, E.: Stable isotope analyses of the pelagic food web in Lake Baikal, *Limnol.*  
798 *Oceanogr.*, 44, 502–511, <https://doi.org/10.4319/lo.1999.44.3.0502>, 1999.
- 799 Zawierucha, K., Buda, J., Pietryka, M., Richter, D., Łokas, E., Lehmann-Konera, S.,  
800 Makowska, N., and Bogdziewicz, M.: Snapshot of micro-animals and associated biotic and  
801 abiotic environmental variables on the edge of the south-west Greenland ice sheet, *Limnology*,  
802 19, 141–150, <https://doi.org/10.1007/s10201-017-0528-9>, 2018.



- 803 Zawierucha, K., Buda, J., Azzoni, R. S., Niškiewicz, M., Franzetti, A., and Ambrosini, R.:  
804 Water bears dominated cryoconite hole ecosystems: densities, habitat preferences and  
805 physiological adaptations of Tardigrada on an alpine glacier, *Aquat. Ecol.*, 53, 543–556,  
806 <https://doi.org/10.1007/s10452-019-09707-2>, 2019a.
- 807 Zawierucha, K., Buda, J., and Nawrot, A.: Extreme weather event results in the removal of  
808 invertebrates from cryoconite holes on an Arctic valley glacier (Longyearbreen, Svalbard),  
809 *Ecol. Res.*, 34, 370–379, <https://doi.org/10.1111/1440-1703.1276>, 2019b.
- 810 Zawierucha, K., Buda, J., Novotna Jaromerska, T., Janko, K., and Gąsiorek, P.: Integrative  
811 approach reveals new species of water bears (*Pilatobius*, *Grevenius*, and *Acutuncus*) from  
812 Arctic cryoconite holes, with the discovery of hidden lineages of *Hypsibius*, *Zool. Anz.*, 289,  
813 141–165, <https://doi.org/10.1016/j.jcz.2020.09.004>, 2020.
- 814 Zawierucha, K., Porazinska, D. L., Ficetola, G. F., Ambrosini, R., Baccolo, G., Buda, J.,  
815 Ceballos, J. L., Devetter, M., Dial, R., Franzetti, A., Fuglewicz, U., Gielly, L., Łokas, E., Janko,  
816 K., Novotna Jaromerska, T., Ko'sci'nski, A., Kozłowska, A., Ono, M., Parnikoza, I., Pittino,  
817 F., Poniecka, E., Sommers, P., Schmidt, S. K., Shain, D., Sikorska, S., Uetake, J., and Takeuchi,  
818 N.: A hole in the nematosphere: tardigrades and rotifers dominate the cryoconite hole  
819 environment, whereas nematodes are missing, *J. Zool.*, 313, 18–36,  
820 <https://doi.org/10.1111/jzo.12832>, 2021.
- 821 Zawierucha, K., Trzebny, A., Buda, J., Bagshaw, E., Franzetti, A., Dabert, M., and Ambrosini,  
822 R.: Trophic and symbiotic links between obligate-glacier water bears (Tardigrada) and  
823 cryoconite microorganisms, *PLoS One*, 17, e0262039,  
824 <https://doi.org/10.1371/journal.pone.0262039>, 2022.
- 825 Zemp, M., Haeberli, W., Hoelzle, M., and Paul, F.: Alpine glaciers to disappear within  
826 decades? *Geophys. Res. Lett.*, 33, L13504, <https://doi.org/10.1029/2006GL026319>, 2006.

